Effect of lattice-mismatch strain on electron dynamics in InAs/GaAs quantum dots as seen by time-domain terahertz spectroscopy

Kojima, Osamu

Izumi, Ryo

Kita, Takashi

(Citation)
Journal of Physics D: Applied Physics,51(30):305102-305102

(Issue Date)
2018-08-01

(Resource Type)
journal article

(Version)
Accepted Manuscript

Effect of lattice-mismatch strain on electron dynamics in InAs/GaAs quantum dots as seen by time-domain terahertz spectroscopy

Osamu Kojima, Ryo Izumi, Takashi Kita

Department of Electrical and Electronic Engineering, Graduate School of Engineering, Kobe University, 1-1 Rokkodai, Nada, Kobe 657-8501, Japan

E-mail: kojima@phoenix.kobe-u.ac.jp

Abstract. Considering the electron dynamics in the deeper area from the surface is important to improve the efficiency of optoelectronic devices. Potential variations due to InAs quantum dot (QD) growth in the GaAs crystal are investigated via measurements of terahertz electromagnetic waves emitted from the surface. In the pump-energy dependence of the time-domain signal, a phase inversion was observed in the QD sample. In addition, while the signal intensity from the InAs QD sample is maintained in the lower pump energy region, the intensity profile does not show this specific change related to the phase inversion. These results demonstrate that the potential change around QDs caused by lattice-mismatched strain can be examined using observations of the time-domain terahertz signal, which can be used to improve the device performance.

PACS numbers: 73.21.La, 78.47.J-, 78.67.Hc

Submitted to: *J. Phys. D: Appl. Phys.*

1. Introduction

Self-assembled quantum dots (QDs) have been extensively studied for various high-efficiency opt-devices, including lasers [1-7], entangled photon sources [8-12], and photovoltaic devices [13-18]. When the efficiency of QD-based devices is considered, variations in the potential structure due to the lattice-mismatched strain, which leads to change in the carrier dynamics, is important. However, it is difficult to directly observe this variation, in particular, around QDs, by the conventional spectroscopy, such as photoluminescence (PL) measurements. For example, even though the bandgap energy of GaAs decreases due to tensile strain at the interface between GaAs and InAs, the experimental observations of variation of the carrier dynamics there are difficult. When the variation of the dynamics can be observed, the device performance can be improved.

On the other hand, observations of terahertz (THz) waves emitted from semiconductor surfaces provide rich information concerning the variation in the structure around the surface [19-22]. Recently, THz devices using semiconductor QDs have been focused [23-27]: therefore, it should be possible to understand the structural variation caused by QD growth using various approaches. In this study, the effects of QD growth on the potential are investigated via observations of THz waves from the GaAs layers. While the fabrication of an InAs QD layer in a GaAs crystal enhances the intensity of the THz wave, the THz signal in the QD sample shows a phase inversion in the pump-energy dependence, which suggests the change in the electron dynamics around the InAs QDs due to the tensile strain. These results indicate that observation of the emitted THz waves from the strained sample can be used to examine the potential modulation due to the strain field. The THz signals measured at various excitation energies are discussed from the perspective of the strain effect.

2. Experiment

The sample used in this study was self-assembled InAs QDs grown on a GaAs (001) substrate by a solid-source molecular-beam epitaxy. After growing a 500 nm buffer layer of GaAs at 550 °C, InAs was deposited at a growth rate of 0.012 ML/s. The deposited InAs layer thickness was 3.6 ML. The average lateral QD length is 40 nm, and the QD density is approximately 1.45×10^{10} /cm^{-2}. QDs on the wetting layer were capped by a 150-nm thick GaAs layer. A GaAs epitaxial film with a thickness of 550 nm on a GaAs substrate was used as a reference. To observe the variation of electron dynamics induced by the QD layer, the larger thickness of epitaxial film than the cap layer was chosen. The thickness of 550 nm can eliminate the contribution of the interface between the film and substrate to the photogenerated carriers generating a THz signal. The measurements of the THz waves were performed out at 297 K using a Ti:sapphire pulse laser with a pulse width of approximately 100 fs. The central energy of the laser pulse was changed from 1.653 eV to 1.425 eV. The pump density was kept at 0.14 μJ/cm^2.

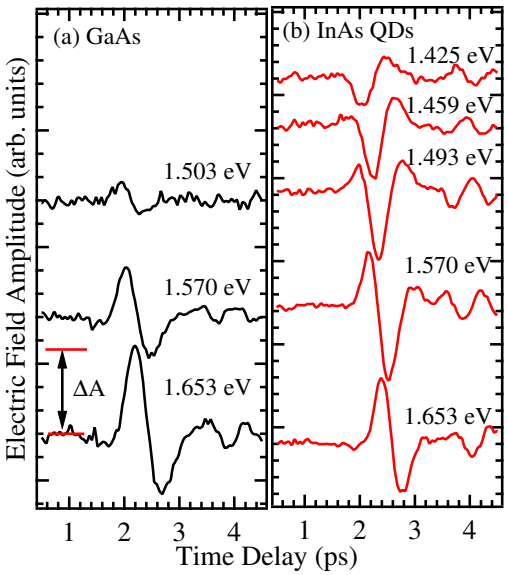

Figure 1. Dependence of the THz signal on the pump energy observed in the (a) reference and (b) QD samples.

Considering the pump-energy dependence measurement, this pump density is almost lowest to obtain the good signal-to-noise ratio signals in our system. The samples were excited by pump pulses at an approximately 45° incidence angle. The THz wave emitted from the samples was collected with a pair of off-axis parabolic mirrors and detected by a commercial photoconductive dipole antenna fabricated on a low-temperature-growth GaAs film (TERA8, Thorlabs).

3. Results and Discussion

Figures 1(a) and 1(b) show the THz signals measured at various pump energies. As shown in Fig. 1(a), while the signal shape measured in the reference sample hardly changes, the amplitude decreases with decreasing excitation energy. This decrease is attributed to the absorption coefficient, that is, decrease in the number of the generated carriers. The signal to noise ratio was too low in the pump energy region less than 1.503 eV to analyze. On the other hand, in the QD sample, shown in Fig. 1(b), the signal shape varies with the pump energy, and the amplitude polarity was completely inverted at 1.459 eV. Moreover, the dependence of the amplitude is different from that of the reference sample.

Here, we focused on the initial rise ΔA of the signals indicated in Fig. 1(a). The values of ΔA for the reference and QD samples are plotted as a function of pump energy in Fig. 2 by the closed and open circles, respectively. The horizontal dotted line indicates $\Delta A = 0$. The polarity inversion, as observed in the QD sample, has been reported in several reports [20, 21, 28-30] and relates to the change in the direction of

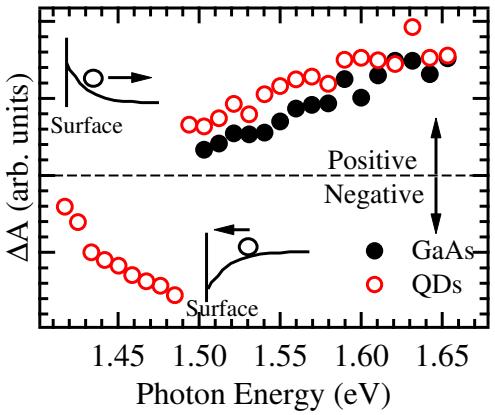

Figure 2. ΔA in the reference and QD samples (the closed and open circles, respectively) plotted as a function of pump energy. The dotted horizontal line indicates $\Delta A = 0$. The inset schmatic of direction of the electron movement.

the dipole. In general, the initial rise is caused by electrons toward the deeper area due to drift and/or diffusion, as shown in the upper inset of Fig. 2. Conversely, the initial intensity drop is caused by the electrons towards the surface, as shown in the lower inset of Fig. 2. Therefore, the inversion of the polarity suggests the change in the direction of the electron movement.

When the origin of change in the polarization direction is considered, the change in the direction of the surface electric field and the change in the doping type cannot be the origin of the polarity inversion because the results at an excitation energy of 1.653 eV show the same polarity direction in both samples; the surface electric field and diffusion coefficient do not depend on the pump energy. Therefore, the mechanism of the phase inversion is different from the previous reports.

If the GaAs surface was modified by the growth of QDs, the PL spectrum of the GaAs layer and the PL excitation (PLE) spectrum detected at the QD PL peak energy shown in Fig. 3(a) will show the specific spectral structure in the region occurring the phase inversion. The arrow in Fig. 3(b) indicates the region measuring the phase-inverted signals. Clearly, in the GaAs PL and QD PLE spectra indicated by the solid curve and open circles, respectively, there was no remarkable point indicating the specific potential structure to explain the phase inversion. The slight difference from the PL spectrum of the reference sample, which was measured the same excitation condition, suggests the strain effects; the increase and decrease in the intensity at the lower and higher energy sides, respectively, originates from the existence of the localized states. In addition, although the absorption coefficient of bulk GaAs increases with the increase in the photon energy [31], the intensity in the PLE signal decreases with increase in the photon energy.

Next, the light intensity profiles in a GaAs crystal were calculated to consider the initial carrier distribution based on the penetration depth of light, as shown in Fig. 4;

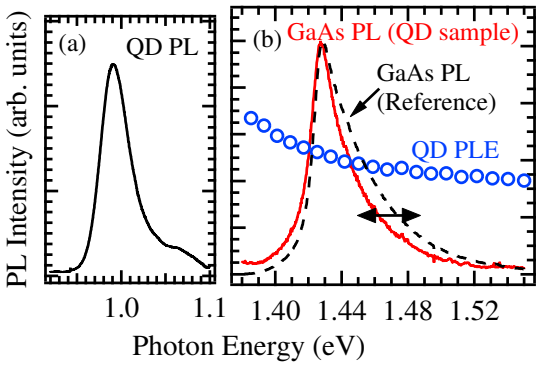

Figure 3. (a) The PL spectrum of QDs. (b) The PL spectrum of GaAs layer observed in the QD sample and the PLE spectrum detected at the PL energy of QDs are indicated by the solid curve and the open circles, respectively. In the region indicated by the arrow, the phase inverted signals were observed. The dashed curve indicates the PL spectrum of the reference sample.

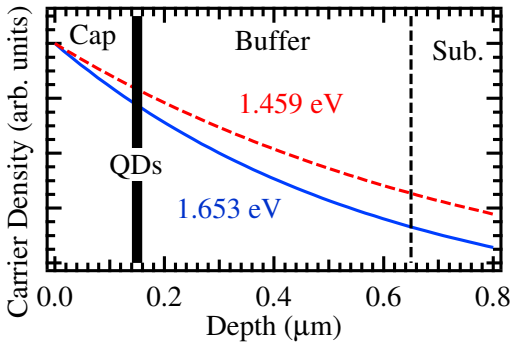

Figure 4. Light intensity profile in GaAs calculated for energies of 1.653 eV and 1.459 eV drawn by the solid and dotted curves, respectively. The vertical solid and dotted lines indicate the positions of the QD layer and the interface of the buffer layer and substrate, respectively.

the solid and dotted curves were calculated using the absorption coefficients at excitation energies of 1.653 eV and 1.459 eV, respectively, in a GaAs crystal [32]. The vertical thick solid and dotted lines indicate the positions of the QD layer and the interface of the buffer layer and substrate, respectively. Considering that the carrier density is proportional to the light intensity, there is no effective difference of the initial electron distribution; the electron diffusion direction from the surface does not change, and the electron always goes to the deeper area. Therefore, the initial carrier distribution is not the origin of the change in the polarization direction.

The results of PL measurements and the calculation of the light intensity profile enables one hypothesis that considering the uniform carrier diffusion from the surface to the deeper area is a problem. Thus, we divided the GaAs region into two parts, the

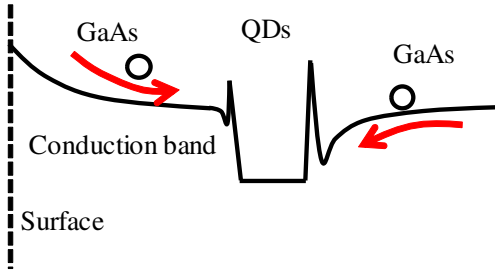

Figure 5. The schematically drawn potential.

cap and buffer layers. As illustrated in Fig. 5, the potential structure is modified by the lattice-mismatched strain; considering the pseudomorphic growth, the tensile strain to GaAs decreases the bandgap energy and the compressive strain to InAs QDs increases the energy. While the ultrafast carrier trap by QDs also modifies the potential [27] and this potential structure is slightly different from the theoretical results [33, 34], in this study, this simplified potential was assumed not to distinct the in-plain and vertical components. Furthermore, the buried InAs QDs are surrounded by the electric field [35-37], which field can be the driving force for the electron drift. According to this potential structure, the electrons generated in the top GaAs layer diffuses to the InAs QDs and mainly contributed to PL. On the other hand, the some of the electrons generated in the bottom GaAs layer diffuses to the substrate, and the rest moves to the InAs QDs, namely, to the surface direction because of the potential gradient. The number of electrons diffusing towards QDs gradually increases with decreasing the excitation energy. Therefore, the potential modification hardly affects to PL.

To demonstrate a gradual increase in the electrons in the buffer layer towards the surface, leading to the gradual phase inversion, the numerical calculation was performed based on the equation shown by Rekaltis [38]. The photocurrent induced by the ultrashort optical pulse is given by

$$J(t) = \frac{4\kappa\kappa_0 m^*}{e\alpha}\left(\frac{eE_0}{m^*}\right)\frac{e^{-\gamma t/2}}{t}\sin\left(\frac{\omega_{\max}+\omega_{\min}}{2}t\right)\sin\left(\frac{\omega_{\max}-\omega_{\min}}{2}t\right), \quad (1)$$

where $\omega_{\max} = \sqrt{\omega_{\rm exc}^2 - \gamma^2/4}$, and $\omega_{\min} = \sqrt{\omega_{\rm exc}^2\exp(-\alpha L_i) - \gamma^2/4}$. $\omega_{\rm exc} = \sqrt{e^2 n_{\rm exc}/\kappa\kappa_0 m^*}$ is the plasma frequency of the photoexcited carriers. κ and κ_0 are the relative permittivity and permittivity of vacuum, respectively. $m^* = 1/(1/m_e + 1/m_h)$ is the reduced mass of an electron-hole pair, $n_{\rm exc}$ is the density of photoexcited electron-hole pairs at the surface, and e is elementary charge.

To divide the calculation into two parts, the photocurrent in the region from the surface to the QD layer and that in the region from the QD layer to the substrate are defined as $J_1(t)$ and $J_2(t)$. For $J_1(t)$, the depletion layer thicknes of $L_i = 150$ nm, which is the thickness of the capping layer, was used. For $J_2(t)$, instead of $n_{\rm exc}$, $n_{\rm exc}\exp(-\alpha L_i)$ ($L_i = 150$ nm) was used to consider the density of photogenerated carrier at the QD-bottom-GaAs. Furthermore, the thickness of the bottom layer of 500 nm was used as

that of the intrinsic layer. In the calculation of $J_2(t)$, to make the direction of electron movement opposite to that of $J_1(t)$, the sign of second sine function was inverted, as follows.

$$J_2(t) \propto \sin\left(\frac{-\omega_{\max} + \omega_{\min}}{2} t\right), \tag{2}$$

This is just mechanical sign innversion. However, in the cases of InAs, InP, and p-type GaAs, which show the negative polarity of the THz signals, the negative polarity can be explained by just changing the sign, phenomenologically. Considering that an important point is the signal consisting of two components; the positive and negative polarities, to express the polarity inversion in the pump-energy dependence, the mechanical change of the sign can be the phenomenologically simplified form. As the calculation paraters, $n_{\rm exc} = 5 \times 10^{16}$ cm^{-3}, $\gamma = 3$ ps^{-1}, $\alpha = 13.52 \times 10^3$ cm^{-1}, $\kappa = 13.559$, $\kappa_0 = 8.854 \times 10^{-12}$ Fm^{-1}, and $E_0 = 10$ kV/cm were used. Here, α for 1.550 eV, κ, $m_e = 0.063 m_0$ and $m_h = 0.51 m_0$ are GaAs parameters mentioned in Ref. [38]. The THz wave forms I_1 and I_2 were numerically calculated as the partial derivative of $J_1(t)$ and $J_2(t)$, respectively. In the calculation, the signal rise was considered by the step function.

The calculation results are shown in Fig. 6. The result of I_1 was indicated by the broken curve, which demonstrates the THz wave signal generated by the carriers in the cap layer. With the increase in the contribution of I_2 to the signal; the contribution of the THz signal caused by carriers in the buffer layer, the sign of signal is inverted. In particular, the gradual inversion is similar to the experimental results. Hence, this result suggests that the phase inversion observed in Fig. 1 originates from variation of the electron dynamics in the buffer layer. The comparison of the calculation with experimental results suggests, while the carriers generated by the higher energy photons hardly supply to QDs, those generated by the lower energy photons supply to QDs. This property supports the PLE spectrum; a slight increase in the PL intensity with decreasing the excitation energy.

Finally, to show the relationship between the THz intensity and phase inversion, the pump-energy dependence of the Fourier transformation (FT) intensity is discussed. A numerical FT was performed for the signals in the time range from 1.5 ps to 4.0 ps in Figs. 1(a) and 1(b). Because the signals were measured without purging, the free induction decay of the water vapor overlaps on the time-domain signal [39]. This effect enhances the intensity of the higher frequency component. Hereafter, we focus on the peak intensity of around 0.8 THz, which is the typical frequency of the THz wave emitted from the GaAs surface.

The FT peak intensities are plotted as a function of pump energy in Fig. 7. The intensity values were normalized by the excitation photon number. The intensity in the reference sample, indicated by the closed circles, monotonically decreases toward the GaAs bandgap energy, indicated by an arrow, with decreasing pump energy. This property agrees with the photon-energy dependence of the absorption coefficient, as mentioned above. Conversely, the intensity in the QD sample, indicated by the open circles, remained in the lower pump-energy region. Characteristics similar to the QD

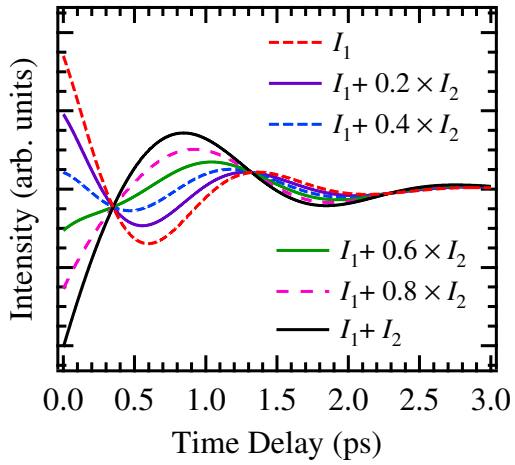

Figure 6. Calculated time domain signals.

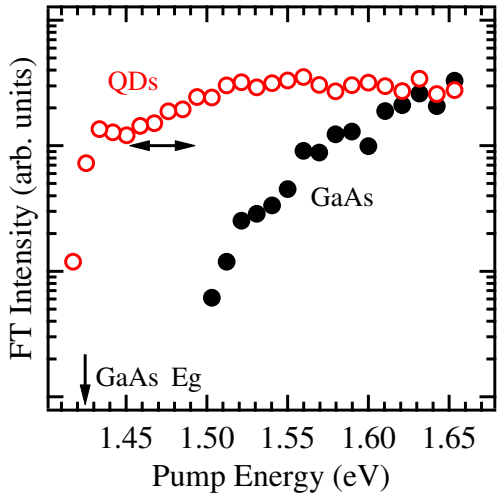

Figure 7. Dependence of the FT intensities for the QD sample and the reference sample, indicated by the open and closed circles, respsectively. An arrow indicates the bandgap energy of GaAs. The double side arrow indicates the region of the phase inversion.

sample were also reported in ref. [25]. Clearly, this intensity profile does not show the possibility causing the modification of the carrier dynamics or some specific features in the energy region indicated by the double side arrow where the phase inversion was observed. These results demonstrate that focusing on the phase of THz time-domain signal is important to find the potential modification due to the strain, which leads to the improvement of the QD devices.

4. Conclusion

We investigated the potential variation caused by QD growth, which is not observed by conventional PL measurements. The dependence of the THz signal on the pump energy in the QD sample shows a phase inversion. This inversion is caused by a potential modulation by the lattice-mismatched strain. In addition, while the QD growth enhances the THz intensity in the lower pump energy region, the intensity profile does not show the possibility of the existence of the modulation. Our results indicate that measurements of the time-domain THz signal could offer the information about the potential change in the deep area, such as underneath of the QD layer, to lead to improve the performance of the semiconductor devices.

Acknowledgments

This work was partially supported by JSPS KAKENHI Grant Numbers of JP26289088 and 16KK0129, and Research Foundation for the Electrotechnology of Chubu.

References

[1] Shoji H.,Nakata Y, Mukai K., Sugiyama Y., Sugawara M., Yokoyama N., and Ishikawa H. 1997 Temperature dependent lasing characteristics of multi-stacked quantum dot lasers *Appl. Phys. Lett.* **71**, 193

[2] Huffaker D. L., Park G., Zou Z., Shchekin O. B. and Deppe, D. G. 1998 1.3 μm room-temperature GaAs-based quantum-dot laser *Appl. Phys. Lett.* **73**, 2564

[3] Salhi A., Fortunato L., Martiradonna L., Cingolani R., De Vittorio M., and Passaseo A. 2006 Enhanced modal gain of multilayer InAs/InGaAs/GaAs quantum dot lasers emitting at 1300 nm *J. Appl. Phys.* **100**, 123111

[4] Liu H., Smowton P., Summers H., Edwards G. and W. Drexler 2009 Self-pulsing 1050 nm quantum dot edge emitting laser diodes *Appl. Phys. Lett.* **95**, 101111

[5] Zhang Z. Y., Oehler A. E. H., Resan B., Kurmulis S., Zhou K. J., Wang Q., Mangold M., Süedmeyer T., Keller U., Weingarten K. J. and Hogg R. A. 2012 1.55 μm InAs/GaAs quantum dots and high repetition rate quantum dot SESAM mode-locked laser *Scientfic Rep.* **2**, 477

[6] Akahane K., Yamamoto N., Kanno A., Inagaki K., Umezawa T., Kawanishi T., Endo T., Tomomatsu Y. and Yamanoi T. 2003 Stable two-mode emission from semiconductor quantum dot laser *Appl. Phys. Express* **6**, 104001

[7] Taylor R. J. E., Childs D. T. D., Ivanov P., Stevens B. J., Babazadeh N., Crombie A. J., Ternent G., Thoms S., Zhou H. and Hogg R. A. 2015 Electronic control of coherence in a two-dimensional array of photonic crystal surface emitting lasers *Scientfic Rep.* **5**, 13203

[8] Fattal D., Inoue K., Vučković J., Santori C., Solomon G. S. and Yamamoto Y. Entanglement formation and violation of bell's inequality with a semiconductor single photon source *Phys. Rev. Lett.* **92**, 037903

[9] Stevenson R. M., Young R. J., Atkinson P., Cooper K., Ritchie D. A. and Shields A. J. 2006 A semiconductor source of triggered entangled photon pairs *Nature* **439**, 179

[10] Chu W. and Zhu J-L 2006 Entangled exciton states and their evaluation in coupled quantum dots *Appl. Phys. Lett.* **89**, 053122

[11] Dousse A., Suffczyński J., Beveratos A., Krebs O., Lemaître A., Sagnes I., Bloch J., Voisin P. and Senellart P. 2010 Ultrabright source of entangled photon pairs *Nature* **466**, 217

[12] Mohan A., Felici M., Gallo P., Dwir B., Rudra A., Faist J. and Kapon E. 2010 Polarization-entangled photons produced with high-symmetry site-controlled quantum dots *Nature Photon.* **4**, 302 (2010).

[13] Aroutiounian V., Petrosyan S., Khachatryan A. and Touryan, K. 2001 Quantum dot solar cells, J. Appl. Phys. **89**, 2268

[14] Martí A., López N., Antolín E., Cánovas E., Luque A., Stanley C. R., Farmer C. D. and Díaz P. 2007 Emitter degradation in quantum dot intermediate band solar cells *Appl. Phys. Lett.* **90**, 233510

[15] Popescu V., Bester G., Hanna M. C., Norman A. G. and Zunger, A 2008 Theoretical and experimental examination of the intermediate-band concept for strain-balanced (In,Ga)As/Ga(As,P) quantum dot solar cells *Phys. Rev. B* **78**, 205321

[16] Guimard D., Morihara R., Bordel D., Tanabe K., Wakayama Y., Nishioka M. and Arakawa Y. 2010 Fabrication of InAs/GaAs quantum dot solar cells with enhanced photocurrent and without degradation of open circuit voltage *Appl. Phys. Lett.* **96**, 203507

[17] Luque A., Martí A. and Stanley C Understanding intermediate-band solar cells, *Nature Photon.* **6**, 146

[18] Asahi S., Teranishi H., Kusaki K., Kaizu T. and Kita T. 2017 Two-step photon up-conversion solar cells *Nature Comm.* **8**, 14962

[19] Zhang X.-C., Hu B. B., Darrow J. T. and Auston, D. H. 1990 Generation of femtosecond electromagnetic pulses from semiconductor surfaces *Appl. Phys. Lett.* **56**, 1011

[20] Birkedal D., Hansen O., Sørensen C. B., Jarasiunas K., Brorson S. D. and Keiding S. R. 1994 Terahertz radiation from delta-doped GaAs *Appl. Phys. Lett.* **65**, 79

[21] Nakajima M., Hangyo M., Ohta M. and Miyazaki H. 2003 Polarity reversal of terahertz waves radiated from semi-insulating InP surfaces induced by temperature *Phys. Rev. B* **67**, 195308

[22] Hwang J. S., Lin H. C., Lin K. I. and Zhang X. C. 2005 Terahertz radiation from InAlAs and GaAs surface intrinsic-N^+ structures and the critical electric fields of semiconductors, *Appl. Phys. Lett.* **87**, 121107

[23] Estacio E., Pham M. H., Takatori S., Cadatal-Raduban M., Nakazato T., Shimizu T., Sarukura N., Somintac A., Defensor M., Awitan F. C. B., Jaculbia R. B., Salvador A. and Garcia A. 2009 Strong enhancement of terahertz emission from GaAs in InAs/GaAs quantum dot structures *Appl. Phys. Lett.* **94**, 232104

[24] Hoffmann M. C., Monozon B. S., Livshits D., Rafailov, E. U. and Turchinovich D. 2010 Terahertz electro-absorption effect enabling femtosecond all-optical switching in semiconductor quantum dots, *Appl. Phys. Lett.* **97**, 231108

[25] Daghestani N. S., Cataluna M. A., Berry G., Ross G. and Rose M. J. 2011 Terahertz emission from InAs/GaAs quantum dot based photoconductive devices *Appl. Phys. Lett.* **98**, 181107

[26] Kruczek T., Leyman R., Carnegie D., Bazieva N., Erbert G., Schulz S., Reardon C., Reynolds S. and Rafailov E. U. 2012 Continuous wave terahertz radiation from an InAs/GaAs quantum-dot photomixer device *Appl. Phys. Lett.* **101**, 081114

[27] Leyman R., Gorodetsky A., Bazieva N., Molis G., Krotkus A., Clarke E., Rafailov E. U., 2016 Quantum dot materials for terahertz generation applications *Laser Photonics Rev.* **10**, 772

[28] Planken P. C. M., Nuss M. C., Knox W. H., Miller D. A. B. and Goossen K. W. 1992 THz pulses from the creation of polarized electron-hole pairs in biased quantum wells *Appl. Phys. Lett.* **61**, 2009

[29] Gu P., Tani M., Kono S., Sakai K. and Zhang X.-C. 2002 Study of terahertz radiation from InAs and InSb *J. Appl. Phys.* **91**, 5533

[30] Hughes J. L., Merchant S. K. E., Fu L., Tan H. H., Jagadish C., Camus E. C. and Johnston M. B. 2006 Influence of surface passivation on ultrafast carrier dynamics and terahertz radiation generation in GaAs *Appl. Phys. Lett.* **89**, 232102

[31] Sturge M. D. 1962 Optical Absorption of Gallium Arsenide between 0.6 and 2.75 eV *Phys. Rev.* **127**, 768

[32] Casey Jr. H. C., Sell D. D. and Wecht K. W., 1975 Concentrate dependence of the absorption coefficient for *n*- and *p*-type GaAs between 1.3 and 1.6 eV *J. Appl. Phys.* **46** 250

[33] Grundmann M., Stier O. and Bimberg D. 1995 InAs/GaAs pyramidal quantum dots: Strain distribution, optical phonons, and electronic structure *Phys. Rev. B* **52**, 11969

[34] Stier O., Grundmann M. and Bimberg D. 1999 Electronic and optical properties of strained quantum dots modeled by 8-band k·p theory *Phys. Rev. B* **59**, 5688

[35] Davies J. H. 1998 Elastic and piezoelectric fields around a buried quantum dot: A simple picture *J. Appl. Phys.* **84**, 1358

[36] Pan E. 2002 Elastic and piezoelectric fields in substrates GaAs (001) and GaAs (111) due to a buried quantum dot *J. Appl. Phys.* **91**, 6379

[37] Jaskólski W., Zieliński M., Bryant G. W., Aizpurua J. 2006 Strain effects on the electronic structure of strongly coupled self-assembled InAs/GaAs quantum dots: Tight-binding approach *Phys. Rev. B* **74**, 195339

[38] Reklaitis A. 2011 Crossover between surface field and photo-Dember effect induced terahertz emission *J. Appl. Phys.* **109** 083108

[39] Harmon S. A. and Cheville R. A. 2004 Part-per-million gas detection from long-baseline THz spectroscopy *Appl. Phys. Lett.* **85**, 2128